A Portable Microwave Scanner for Brain Stroke Monitoring: Design, Implementation and Experimental Validation

D. O. Rodriguez-Duarte*, J. A. Tobon Vasquez*, S. de Luque Arias*, R. Scapaticci†, L. Crocco†, F. Vipiana*
*Dept. Electronics and Telecommunications, Politecnico di Torino, Torino, Italy,
{david.rodriguez, jorge.tobon, francesca.vipina}@polito.it
†Institute for the Electromagnetic Sensing of the Environment, National Research Council of Italy, Naples, Italy,
{scapaticci.r, crocco.l}@irea.cnr.it

***Abstract*—This paper presents the design, the realization, and the experimental assessment of a novel portable microwave scanner prototype for brain stroke monitoring. The device employs a 22-antenna-array, placed conformal to the upper head part, composed of compact, flexible, and custom-made antennas working at around 1 GHz. The validation includes the monitoring of an experimentally emulated evolving hemorrhagic stroke. The progression of the medical condition is emulated via a non-static phantom (custom-shape balloon), derived from medical images, and a single-cavity 3-D anthropomorphic head phantom. The phantoms are filled with liquids mimicking the dielectric properties of the hemorrhage and the average brain tissues, respectively. The imaging-based follow-up is approached using a differential scheme that receives the scattering matrices, taken at two different instants, and exploits the distorted Born approximation to form the image in real-time. The kernel of the imaging algorithm is computed through accurate numerical models. The results verify the capabilities of the system to assess the continuous evolution of the stroke.**

***Index Terms*—Microwave imaging, biomedical imaging, microwave antenna array, flexible antenna, hemorrhagic stroke, numerical simulation, propagation.**

I. Introduction

A stroke is a critical medical condition that provokes the death of millions of neurons per minute, causing post-onset long-life disabilities or even the patient's death. It occurs when a clot or a burstof an artery within the brain deteriorates the brain's normal flow of rich-oxygen blood. The extend of the stroke-affected region varies depending on the infarct severity and the time of diagnosis, typically being between 2 to 200 cm^3 [1], [2]. The growth of the stroke is faster in the first hours after its onset, showing a slight variation after 72 hours. The outcome of the stroke, patient functional status after the attack, depends on multiple variables such as the location or pre-medical conditions. However, clinical studies have found that patients with an initial infarct volume less than 80 cm^3 have a more favorable outcome than larger ones [3], [4]. Thus, instruments that determine the shape, location and size are valuable support for the prognosis and the therapeutic assessment for the physicians. To address these needs, several imaging modalities have been developed and magnetic resonance imaging (MRI) and computerized X-ray tomography (CT) represent the gold standard imaging-based technologies used as diagnostic tools to produce reliable clinical information.

On the other hand, continuous physiological monitoring in the stroke post-acute stage is also important to promptly update the administered therapies and improve their effectiveness. However, MRI and CT are unviable for continuous follow-up, due to their inherent limitations regarding the portability, cost and harmful effects (in the case of CT) . In fact, such a monitoring task especially during the first two days after the onset, is currently associated with improved outcomes and the prevention of further complications [5]. For this reason, there is a clear need for alternative imaging technologies capable to achieve this goal.

In this respect, microwave imaging (MWI) represents an attractive alternative. It is a technology with good-performing penetration, dielectric sensitivity, non-invasiveness, safety (non-ionizing and low-power nature of the employed radiations), and cost [6], [7]. The MWI principle relies on the contrast of the electromagnetic properties (permittivity and conductivity) existing between the different tissues within the domain of imaging (DOI), e.g., the healthy brain tissues and the injured areas in the stroke monitoring case. This contrast gives raise to a scattered field that, properly process through the solution of an inverse scattering problem, provides a map of the electromagnetic properties of the DOI.

Recently, different devices focused on the imaging of brain stroke are being developed at an industrial and academic level. From the industrial side, there are found three remarkable examples. First, the "Strokefinder" , from Medfield Diagnostics [8], is a device focused on the stroke-typology classification as decision-support to assist in clinical evaluation. Second, the "BrainScanner", from EMTensor [9], that provides 24/7 in-hospital head scanning. Third, The "EMVT" , from EMVision

This work was supported by the Italian Ministry of University and Research under the PRIN project "MiBraScan", and by the European Union's Horizon 2020 research and innovation program under the EMERALD project, Marie Skłodowska-Curie grant agreement No. 764479.

[10], which is in clinical testing. Those devices reaffirm the potential of the technology, though, also open the door to new developments as lower complexity devices.

On the other hand, from academia, the King's College London group developed a device with an 8-antenna array submerged in glycerine as a matching medium, performing a 2-D tomography [11]. Similarly, in [12], a 2-D tomographic approach and an 16-antenna array ring surrounding the head are employed. In this last, the matching medium consist of heat-sealed polyethylene bags filled up with a water-glycerine-based liquid. Also, the University of Queensland group works on different prototypes. For instance, in [13], it is showed a ring of 14-antenna array and a novel polar sensitivity encoding (PSE) to locate the stroke. Also, more recently, in [14], a flexible-24-antenna cap and 3-D tomography imaging technique have been proposed, achieving the location of the stroke in complex scenarios, yet with limited shape retrieval and non-monitoring testing. Furthermore, some of the authors of this work have presented a functional prototype using an array of brick-shaped but unpractical at the clinical environment due to its dimensions and weigh [15], [16].

In this paper, a new low-complexity device prototype for 3-D brain stroke monitoring is presented. As compared to previous devices [15], [16], the one presented herein fully meets the requirement of portability, being based on a custom-made array of low-weight flexible antennas. Moreover, thanks to a distribution of the array elements conformal to the head, the proposed device further scales down the overall complexity, as it only exploits 22 antennas.

Besides describing the features of the device, an experimental validation of its imaging capabilities in monitoring emulated hemorrhagic conditions is reported. Such a challenging clinical condition is implemented introducing a non-static realistic stroke phantom obtained from the segmentation of medical images (CT scans), and in-house manufactured. Such a non-static target is used to validate the early-stage stroke follow-up capabilities of the system, monitoring a growth from 5 to 15 cm3. To the best of the authors knowledge, the results herein presented provide the first experimental validation of dynamic monitoring in a true-to-life scenario mimicking brain stroke.

II. Materials and Methods

A. Microwave Imaging Prototype

This section describes the hardware components of the proposed MWI scanner, focusing on the elements involved in the signals flow from the antennas' port until the imaging processing unit. The radiating part of the system is described in Sect. II-B.

The first element is the Vector Network Analyzer (VNA). It generates the stimulus signals injected and captures the backscattered signals. The second component is the switching matrix, that multiplexes and drives the transmitted and received signals the VNA 2-port to the 22 port of the antenna modules. Finally, the last component is a laptop that controls the switching and collects the data. For this prototype, we are

Fig. 1. Microwave brain imaging system prototype: (A) vector network analyzer, (B) DC power source, (C) switching matrix, (D) head phantom and antennas.

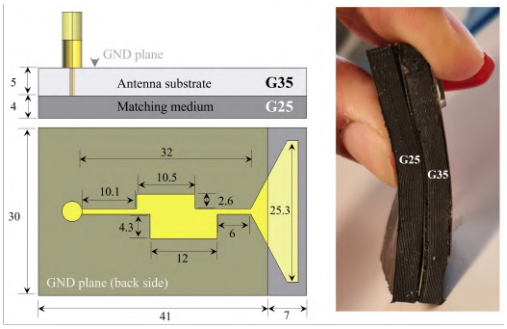

Fig. 2. (Left): antenna diagram with all dimensions in mm; (right): lateral view with bending.

using a compact 2-port P9375A Keysight Streamline USB VNA [17] and a switching matrix that combines single-pole-four-throw (SP4T), single-pole-six-throw (SP6T), and single-pole-double-throw (SPDT) electromechanical coaxial switches [18]. Hence, each antenna is connected to its respective switch via a flexible coaxial cable. Figure 1 shows an overview of the system.

B. Antenna Design and Realization

To reduce the size and weight of the device a novel compact antenna design optimized to work on the proximity of a human head has been designed and realized, taking as starting point the brick-shaped antenna in [19]. The antenna consists of two stacked layers of custom flexible dielectric material with a circuit-printed low-complexity monopole in between and back-fed via a coaxial connector, as shown in Fig. 2. The first layer serves as the traditional substrate of the printed antennas, but in this case, it is made of a customizable material. The substrate then supports on the backside the antenna ground (GND) plane and a printed triangular radiator on the front side, which are printed on flexible commercial 50 µm-thickness polyimid film. The second layer is also a dielectrically customizable medium that reduces the mismatch between the antenna and the head. Thus, the custom layers are tuned to find a good trade-off between high permittivity and low losses and are made with a urethane rubber and graphite powder mixture. Table I presents the weight percentage to obtain both layers, called G35 and G25, and their dielectric properties, respectively.

The substrate, the matching medium, and the printed monopole make an antenna module, which reaches enough flexibility to adapt to the head curvature. This module is

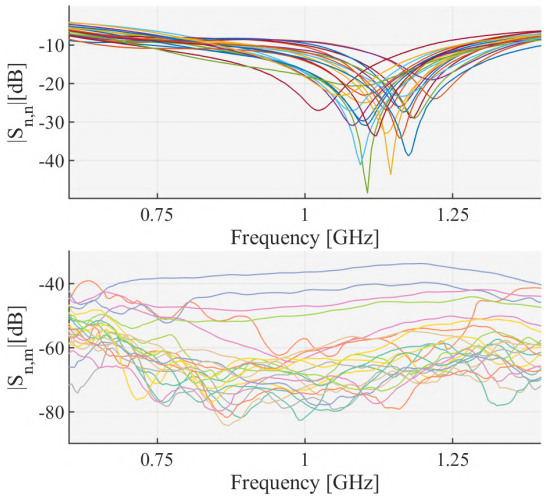

Fig. 3. S-parameters amplitude; (Top): reflection coefficients, each line corresponds to the $|S_{n,n}|$ in dB for the n-th antenna of the MWI system with $n = 1, \ldots, 22$; (bottom): transmission coefficients, each line corresponds to the $|S_{m,n}|$ in dB with $n = 1$ (transmitting antenna) and $m = 2, \ldots, 22$ (receiving antennas).

TABLE I
MATERIALS COMPOSITION AND PERMITTIVITY

	Triton X-100[%]	Water [%]	Salt [g/l]	ϵ_r (1 GHz)	σ [S/m]
ICH	14	86	9.4	68	1.5
Brain	38	62	5.2	45	0.7
	Graphite [%]	Rubber [%]	–	ϵ_r (1 GHz)	σ [S/m]
Matching	75	25		13	0.18
Substrate	65	35		18	0.3

optimized to work in a -10 dB band from 0.85 to 1.25 GHz (see Fig. 3), suitable in terms of penetration and resolution for the application [20]. Hence, the proposed module joins the benefits of a flexible antenna with low cost, low complexity, and modularity. In other words, a modular scheme allows to scale or upgrade a system efficiently and easily maintain/repair the system.

We choose a 22-antenna configuration for the MWI scanner, placing the modules conformally to the upper part of the head, following the rigorous design procedures described in [20]. Moreover, it is verified that the transmission values among all the antenna pairs are well above the VNA noise floor, as shown in bottom of Fig. 3.

C. The Head and Stroke Phantoms

To mimic a realistic and meaningful pathological condition, an ad-hoc anthropomorphic phantom has been developed. The phantom is made of a static part and a dynamic part. The static part of the phantom has the twofold purpose of modeling the head of a human adult and providing a support for the antenna array, i.e., the helmet containing the antennas. The head is shaped taking as reference the MRI-derived anthropomorphic phantom in [21] and consists of a 3-D printed 3 mm-thick single-cavity container made of clear resin (polyester casting resin) parts, which are then glued and assembled. Moreover, individual antenna supports are printed on the outer upper part of the head, thus, facilitating the maintenance and reducing the positioning uncertainties.

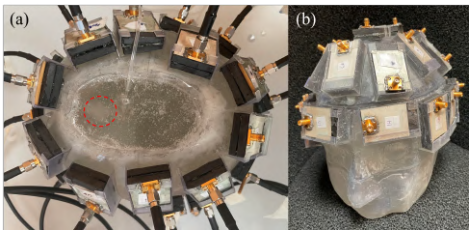

Fig. 4. Photo of head phantom and antenna array. (a): Top view, the red circle indicates the position of the stroke; (b): isometric view.

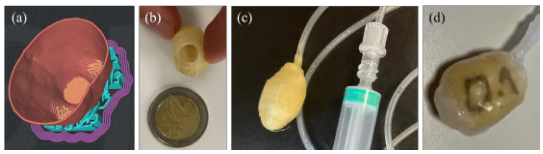

Fig. 5. Stroke phantom manufacturing. (a) 3-D model cut view; (b) PVA mold; (c) Model sealed; (d) Stroke phantom before of remove PVA material.

The non-static phantom is developed to provide a simplified model of the stroke. To realize it, a real stroke shape has been obtained segmenting CT medical images. This realistic shape has been 3-D printed using a PVA 3D filament [22], setting the printer to the minimum thickness extrusion (around 0.1 mm) and the number of layers by thickness to one (see Fig. 5a). Then, the printed PVA mold has been coated with a thin (less than 1 mm) slow-cure platinum silicone layer [23] and let it rest for some hours. Finally, water has been injected into the obtained phantom to dissolve the PVA, removing the residues through a small hole with a syringe. As shown in Fig. 5, the final result is a multi-use, flexible, and resistant stroke phantom sealed and attached to a 3mm-radius feeding cannula.

Finally, each phantom is filled using liquids that mimic the electrical properties of the hemorrhagic stroke and the average brain. The bottom part of Table I summarizes the recipe used to obtain both materials, dubbed them as “ICH” (Intracraneal hemorrhagic) and “Brain”. It also presents the corresponding values of permittivity and conductivity at 1 GHz, measured using the open probe technique (see further details in [16]).

D. The Imaging Algorithm

The data measured by the device are processed with the same approach as in [15], [16] to allow real-time results. The input of the imaging procedure is the differential scattering matrix ΔS obtained by subtracting the scattering matrices measured at two different instants, say t_0 and t_1. The output is a map contrast variation occurring between t_0 and t_1,

$$\Delta\chi(t_0, t_1) = \frac{\epsilon(t_1) - \epsilon(t_0)}{\epsilon_b}, \tag{1}$$

where $\epsilon(t_0)$ and $\epsilon(t_1)$ are the complex permittivities, and b stands for the background scenario. Assuming that the change

in the stroke at t_1 only induces a weak perturbation of the scenario at t_0, the functional relationship between the input and the output of the imaging algorithm can be modeled via the Born approximation as

$$\Delta S(t_0, t_1) = -\frac{j\,\omega\,\epsilon_b}{2\,a_p\,a_q} \int_D \mathbf{E}_p(t_0) \cdot \mathbf{E}_q(t_0)\,\Delta\chi\,d\mathbf{r}, \quad (2)$$

where the symbol "$\cdot$" denotes the dot product between vectors, j is the imaginary unit, $\omega = 2\pi f$ is the angular frequency, and a_p and a_q are the known incoming root-power waves at the p and q antenna ports, respectively [6]. $\mathbf{E}_p(t_0)$ and $\mathbf{E}_q(t_0)$ represent the nominal electric field, i.e., the field in the initial conditions, radiated in the DOI in healthy conditions by the p-th and q-th array element respectively. Such a fields are obtained via full-wave simulation of a virtual twin [15], [25], employing an in-house Finite Element Method EM solver [26].

Equation 2 is inverted in a regularized form by means of the truncated singular value decomposition (TSVD) scheme [24], which provides the explicit inversion formula:

$$\Delta\chi = \sum_{n=1}^{T} \frac{1}{\sigma_n} \langle \Delta S, u_n \rangle\, v_n, \quad (3)$$

where $\langle u, \sigma, v \rangle$ is is the SVD of the discretized counterpart of the integral operator at the right hand side of Eq. 2 and T is the truncation index that acts as a regularization parameter set as -25 dB.

Finally, the normalized modulus of the retrieved differential contrast is given as final output of the procedure.

E. Experimental Procedure

For the experiments, the stroke phantom presented previously has been placed in the back part of the head around the occipital and parietal zone of the brain, a medical condition that provokes the malfunction of the visual system causing cortically-induced blindness [4]. The stroke model is introduced from the upper part of the head phantom and filled then in a controlled manner using a cannula and a syringe reaching four different states, i.e., empty stroke (healthy), 5 cm^3, 10 cm^3, and 15 cm^3, as shown in Fig. 6.

At each state, the scattering parameters are measured, avoiding undesired disturbances unavoidably arising if the phantom should have been removed from the head. For the measurements, the VNA has been set with an input power of -5 dBm and the intermediate filter (IF) to 100 Hz, reaching a good compromise between the noise floor, around -100 dB. The time required to measure a full set of scattering parameters is about 5 minutes, but it is worth noticing it can be significantly reduce by replacing electromechanical switches with solid state ones.

III. Experimental Results

The measured data provide three differential scattering matrices $\Delta S = S(t_0) - S(t_s)$, where s indicates the measured set, $s = 0$ refers to healthy or empty stroke, $s = 1$ to 5 cm^3 stroke volume, s =2 to 10 cm^3, and $s = 3$ to 15 cm^3. The three matrices at 1 GHz are shown in the top row of Fig. 7 and referred to as I, II and III, respectively.

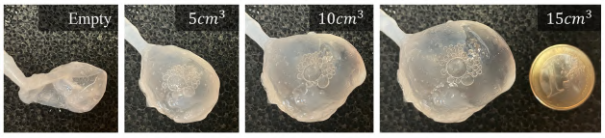

Fig. 6. Photo of the non-static stroke phantom growth. From left to right: Empty, 5 cm^3, 10 cm^3, and 15 cm^3

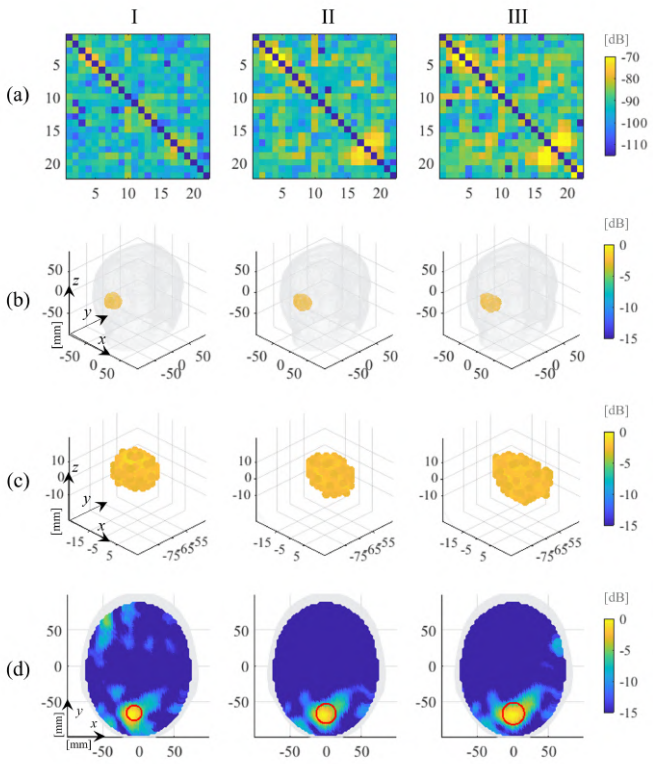

Fig. 7. Scenarios I(0-5 cm^3), II(0-10 cm^3) and II(0-15 cm^3). (a) Differential scattering matrices; (b) normalized reconstructed dielectric contrast values above -3 dB; (c) zooming up of row b; (d) transverse view center at the maximum, amplitude normalized of the reconstructed dielectric contrast. The red circles indicate the contour of the spheres with the volume of 5, 10 and 15 cm^3, respectively.

The obtained 3-D images of the evolving stroke are reported in the second row of Fig. 7. For the sake of readability the normalized amplitude of the reconstructed differential contrast is binarized by setting to zero the voxel below -3 dB. Fig. 7(c) is a zoom-up of (b) in the stroke region, while Fig. 7(d), shows the transverse cut of the reconstructed differential in the plane where it attains its maximum value. Moreover, we add as visual reference three red circles (center at the maximum of each scenario) with radii 10.6, 13.7 and 15.3 mm, corresponding respectively to spheres of volume 5 ,10 and 15 cm^3.

From the results illustrated in Fig. 7, it can be appreciated that the system is capable of localize the pathology in all cases, achieving (with respect to the expected values) a good estimation of the shape and size, with an error in the order of half centimeter. Moreover, it clearly appears that the device is

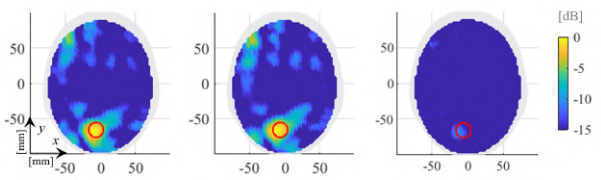

Fig. 8. Transverse views center at the maximum, amplitude normalized of the reconstructed dielectric contrast. (from left to right) Reference scenario 5 cm^3(See Fig.7(I-d)); Scenario 5 cm^3 using a different set of measurements; false-positive scenario, difference between two empty cases normalized at maximum value of I-d. The red circles indicate the contour of the sphere with the volume of 5 cm^3.

able to track the change of the stroke shape.

Finally, as a further test and validation, a repeatability test and a false-positive test have been carried out. These test are summarized in Fig. 8. For the repeatability test, case I has been performed twice using different sets of measurements for both the empty and 5 cm^3 conditions. As can be seen, in the leftmost and central panel of Fig. 8 the achieved results are almost identical. For the false-positive test, the differential S matrix obtained by subtracting two empty cases has been processed. The obtained image normalized to the maximum reference scenario (case I) is shown in the rightmost panel of Fig. 8 and shows that it is possible to discriminate this condition as well.

IV. Conclusion and Perspectives

In this paper, a new microwave scanner designed for brain stroke monitoring has been presented. The device meets the requirements in terms of low complexity and portability by resorting to a 22-elements array of custom designed flexible antennas and its imaging capabilities have experimentally assessed in realistic clinical conditions. In particular a time-changing scenario has been mimicked by means of an ad-hoc realized non-static anthropomorphic phantom.

Future work aims at extending the validation of the system in other relevant conditions and further improve the imaging results by exploiting multifrequency data.

Acknowledgment

We thank Prof. N. Joachimowicz, Sorbonne University, and Prof. P. Plaisance and Eng. V, Lemarteleur, Ilumens Health Simulation Center, for providing the medical images and the fruitful discussions on the medical aspects and on the modeling manufacturing of the phantoms.

References

[1] C. Laredo, Y. Zhao, S. Rudilosso, A. Renu, J.C. Pariente, et al., "Prognostic Significance of Infarct Size and Location: The Case of Insular Stroke," *Sci. Rep.*, vol.8, 2018, doi:10.1038/s41598-018-27883-3.

[2] A. Bruno, N. Shah, A.E. Akinwuntan, B. Close and J.A. Switzer, "Stroke size correlates with functional outcome on the simplified modified Rankin Scale questionnaire," *J. Stroke Cerebrovasc. Dis.*, vol.22, pp. 781-783, 2013, doi:10.1016/j.jstrokecerebrovasdis.2012.03.011.

[3] D.E. Saunders, A.G. Clifton and M.M. Brown, "Measurement of Infarct Size Using MRI Predicts Prognosis in Middle Cerebral Artery Infarction," *J. Stroke*, vol.26, no. 12, pp. 2272-2276, 1995, doi:10.1161/01.STR.26.12.2272.

[4] E.L. Saionz, D. Tadin, M.D. Melnick and K.R. Huxlin, "Functional preservation and enhanced capacity for visual restoration in subacute occipital stroke," *Brain*, Vol. 143, no. 6, pp.1857–1872, 2020, doi:10.1093/brain/awaa128.

[5] A. Ciccone, M.G. Celani, R. Chiaramonte, C. Rossi and E. Righetti, "Continuous versus intermittent physiological monitoring for acute stroke," in Cochrane Database of Systematic Reviews 2013, Issue 5, no.CD008444. doi:10.1002/14651858.CD008444.pub2

[6] N. K. Nikolova, Introduction to Microwave Imaging. Cambridge: Cambridge University Press, 2017.

[7] L. Crocco, I. Karanasiou, M. James, R. Conceição (eds), Emerging Electromagnetic Technologies for Brain Diseases Diagnostics, Monitoring and Therapy. Springer, 2018

[8] "Medfield." Available at https://www.medfielddiagnostics.com/en/.

[9] "EMTensor." Available at https://www.emtensor.com/.

[10] "EMVision." Available at https://emvision.com.au/.

[11] O. Karadima, M. Rahman, J. Sotiriou, N. Ghavami, P. Lu, S. Ahsan, and P. Kosmas, "Experimental validation of microwave tomography with the DBIM-TwIST algorithm for brain stroke detection and classification," *SENSORS*, vol. 20, Feb. 2020.

[12] A. Fedeli, C. Estatico, M. Pastorino, and A. Randazzo, "Microwave detection of brain injuries by means of a hybrid imaging method," *IEEE Open Journal of Antennas and Propagation*, pp. 1–11, 2020.

[13] A. Trakic et al., "Expedited Stroke Imaging With Electromagnetic Polar Sensitivity Encoding," *IEEE Transactions on Antennas and Propagation*, vol. 68, no. 12, pp. 8072-8081, Dec. 2020, doi: 10.1109/TAP.2020.2996810.

[14] A. S. M. Alqadami, A. Zamani, A. Trakic and A. Abbosh, "Flexible Electromagnetic Cap for Three-Dimensional Electromagnetic Head Imaging," *IEEE Transactions on Biomedical Engineering*, vol. 68, no. 9, pp. 2880-2891, Sept. 2021, doi: 10.1109/TBME.2021.3084313.

[15] J. A. Tobon Vasquez et al., "A Prototype Microwave System for 3D Brain Stroke Imaging," *Sensors*, vol. 20, no. 9, May 2020, doi: 10.3390/s20092607.

[16] D. O. Rodriguez-Duarte, J. A. Tobon Vasquez, R. Scapaticci, G. Turvani, M. Cavagnaro, M.R. Casu, L. Crocco and F. Vipiana, "Experimental Validation of a Microwave System for Brain Stroke 3-D Imaging," *Diagnostics*, vol. 11, no. 7, 2021, doi: 10.3390/diagnostics11071232.

[17] Keysight Technologies.Keysight Streamline Series USB Vector Network Analyzer P937XA 2-port, up to 26.5 GHz. *Data Sheet Tech. Specif.* 2018.

[18] J. A. Tobon Vasquez, R. Scapaticci, G. Turvani, G. Bellizzi, N. Joachimowicz, B. Duchene, E. Tedeschi, M. R. Casu, L. Crocco, F. Vipiana, "Design and Experimental Assessment of a 2-D Microwave Imaging System for Brain Stroke Monitoring", *Int. Journal of Antennas and Propagation, Special Issue on Bioengineering Applications of EM Wave Propagation*, Article ID 8065036, 12 pages, 2019, doi:10.1155/2019/80650362019.

[19] D. O. Rodriguez-Duarte, J. A. Tobon Vasquez, R. Scapaticci, L. Crocco and F. Vipiana, "Brick Shaped Antenna Module for Microwave Brain Imaging Systems," *IEEE Antennas and Wireless Propagation Letters*, vol. 19, no. 12, Dec. 2020, pp. 2057-2061, doi: 10.1109/LAWP.2020.3022161.

[20] R. Scapaticci, J. Tobon, G. Bellizzi, F. Vipiana and L. Crocco, "Design and Numerical Characterization of a Low-Complexity Microwave Device for Brain Stroke Monitoring," *IEEE Transactions on Antennas and Propagation*, vol. 66, no. 12, pp. 7328-7338, Dec. 2018, doi: 10.1109/TAP.2018.2871266.

[21] N. Joachimowicz, B. Duchene, C. Conessa, and O. Meyer, "Anthropomorphic breast and head phantoms for microwave imaging," *Diagnostics*, vol. 85, pp. 1–12, Dec. 2018.

[22] "Esun." Available at https://www.esun3d.net/Products/PVA.

[23] "Smooth-on." Available at https://www.smooth-on.com/product-line/dragon-skin/.

[24] M. Bertero and P. Boccacci, Introduction to Inverse Problems in Imaging. Inst. Phys., Bristol, U.K., 1998.

[25] D. O. Rodriguez-Duarte, J. A. Tobon Vasquez, R. Scapaticci, L. Crocco and F. Vipiana, "Assessing a Microwave Imaging System for Brain Stroke Monitoring via High Fidelity Numerical Modelling," *IEEE Journal of Electromagnetics, RF and Microwaves in Medicine and Biology*, vol. 5, no. 3, pp. 238-245, Sept. 2021, doi: 10.1109/JERM.2020.3049071.

[26] E. A. Attardo, A. Borsic, G. Vecchi and P. M. Meaney, "Whole-System Electromagnetic Modeling for Microwave Tomography," *IEEE Antennas and Wireless Propagation Letters*, vol. 11, pp. 1618-1621, 2012, doi: 10.1109/LAWP.2013.2237745.